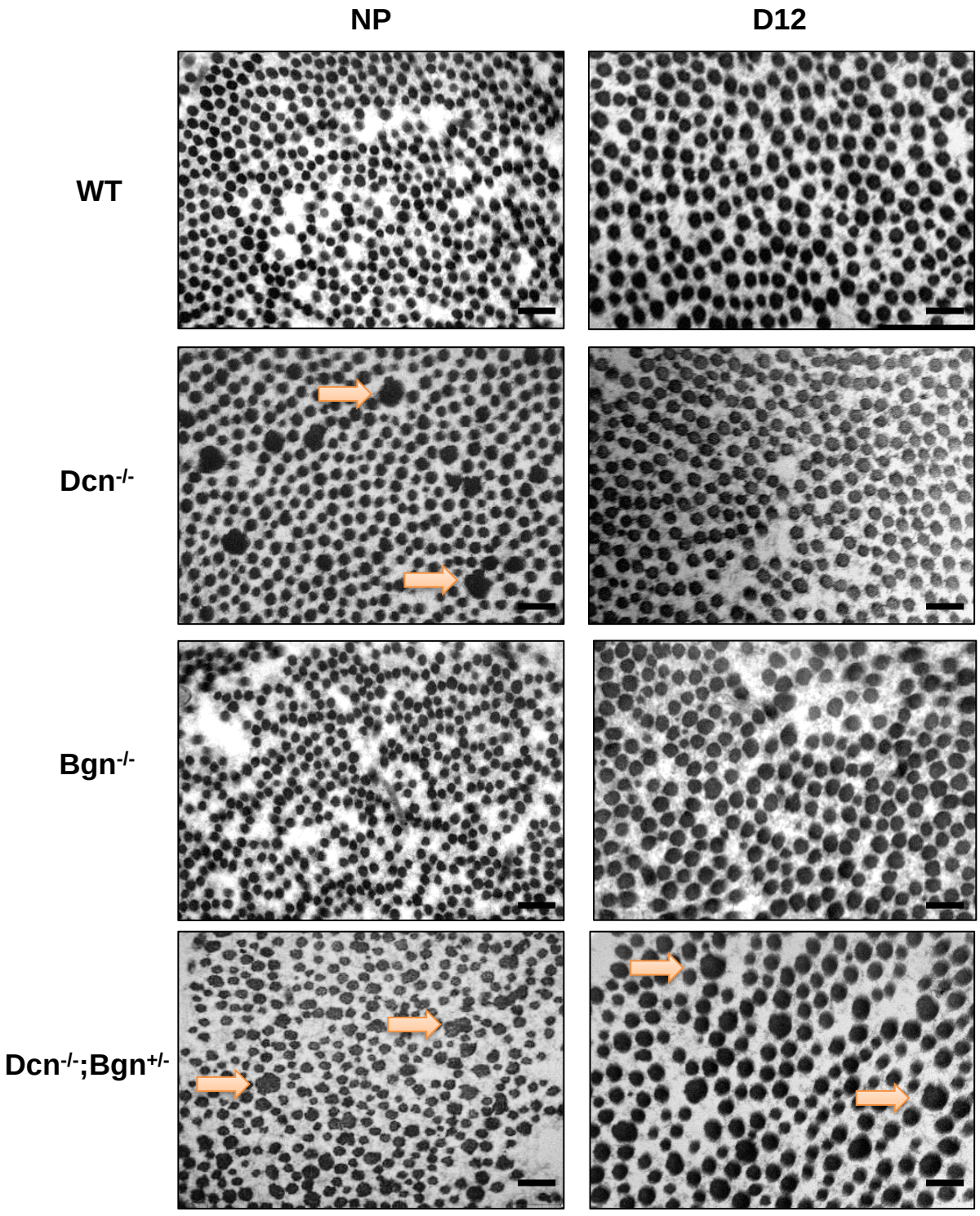

Supplementary Figure 1: Defects in collagen fibrils are sustained in the Dcn$^{-/-}$;Bgn$^{+/-}$ mice until mid-pregnancy. TEM images identify abnormal collagen fibrils (depicted by the orange arrow) in the NP Dcn single KO (Dcn$^{-/-}$) and Dcn$^{-/-}$;Bgn$^{+/-}$ cervices (left panel). Collagen defects were sustained in the subepithelial region of Dcn$^{-/-}$;Bgn+/- but not single KO through gestation day 12 (right panel) after which these abnormal fibrils were resolved in gestation day 18 (Figure 4). n= 3 animals per genotype and time point. Scale bars, 500 nm.

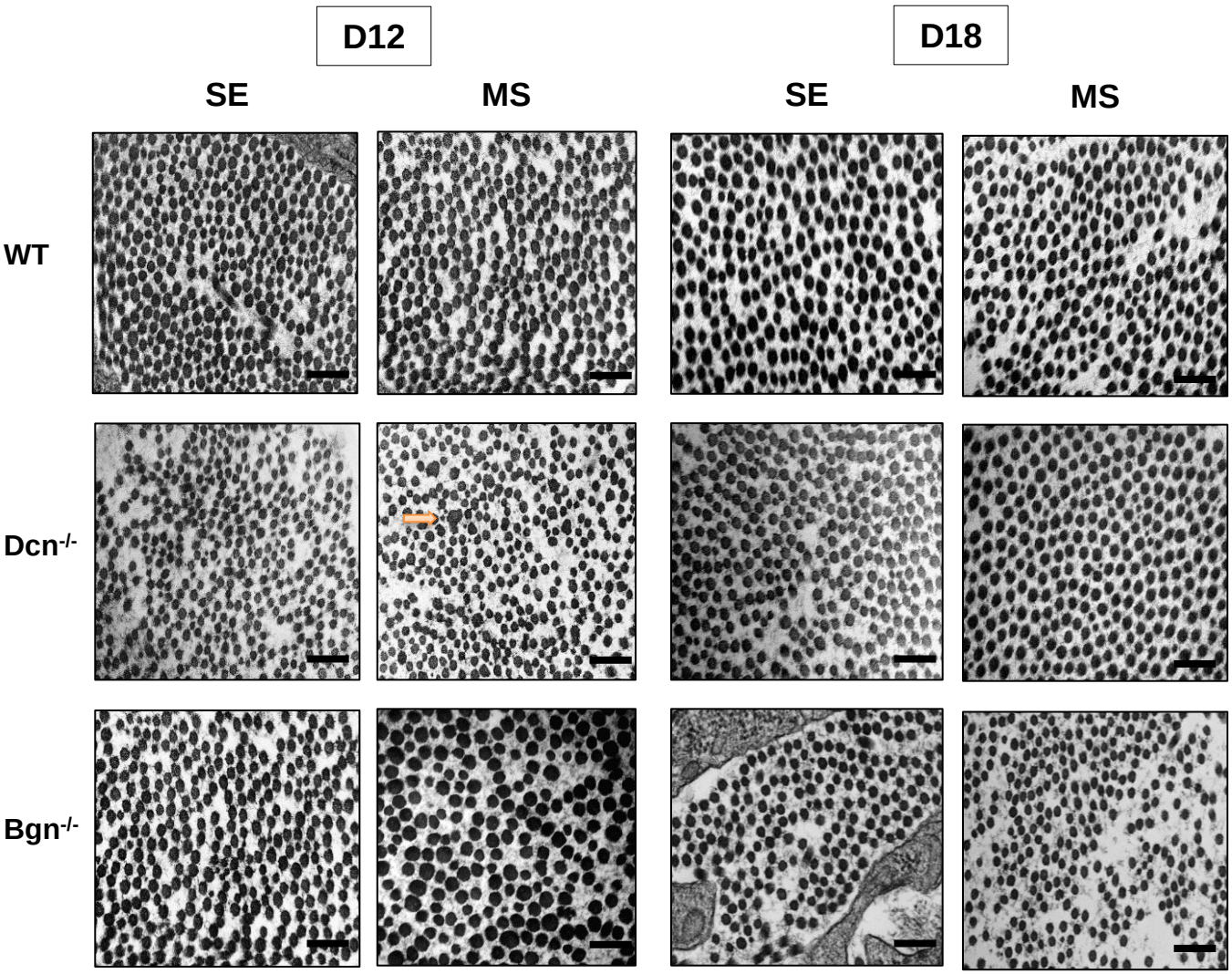

Supplementary Figure 2: **A spatial pattern of collagen reorganization is also seen in Dcn$^{-/-}$ cervix.** TEM analysis in Dcn$^{-/-}$ identify defects in collagen fibrils structure (as shown by the orange arrow) in the MS region on day 12 and these abnormalities were completely resolved in the MS region by the end of pregnancy (day 18). No defects in collagen fibrils were observed in SE and MS regions in the WT or the Bgn$^{-/-}$ cervices. n= 3 animals per genotype and time point. Scale bars, 500 nm.

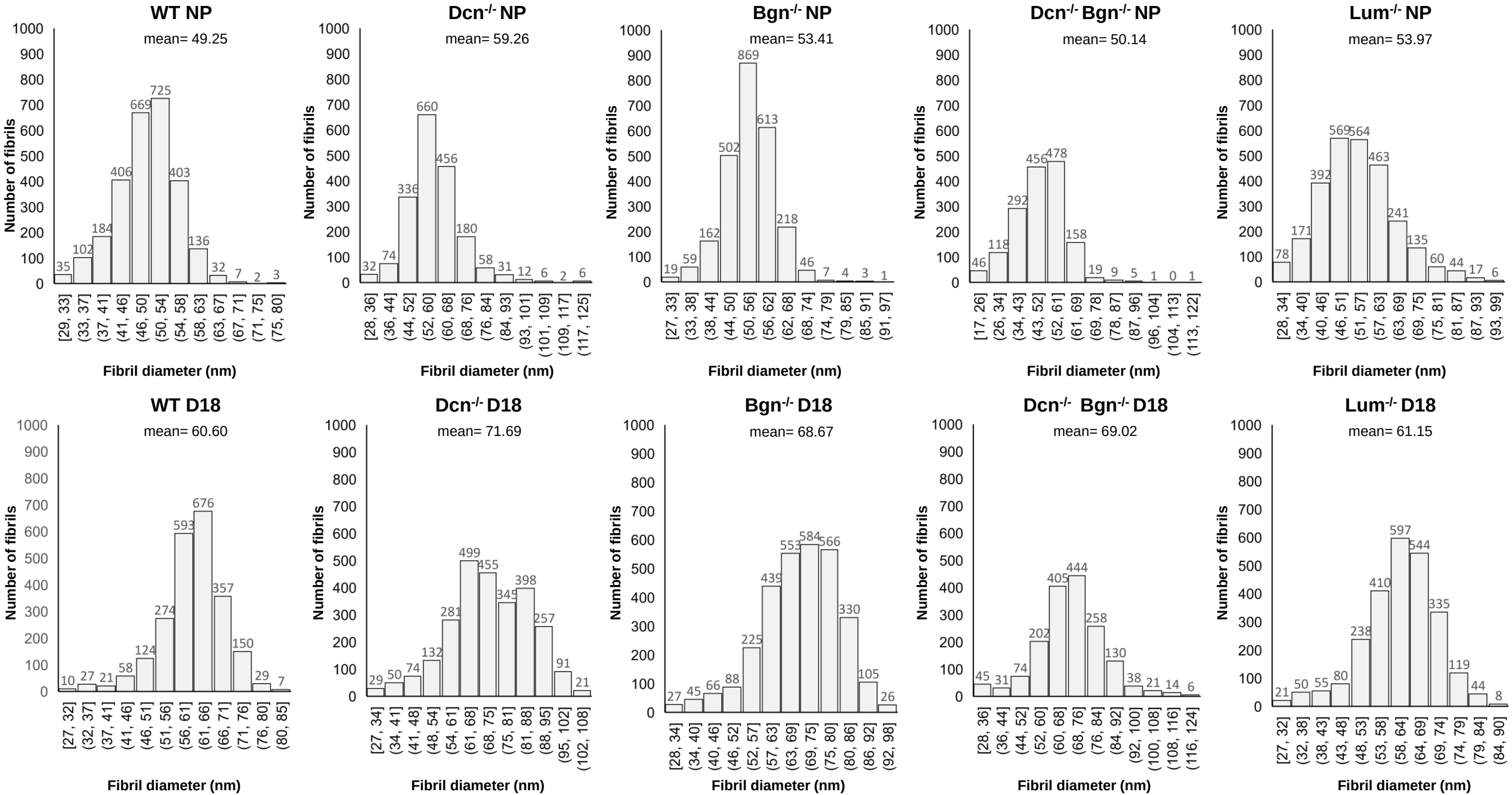

Supplementary Figure 3: Number of collagen fibrils in the cervical ECM of class I and class II SLRPs. Tissue electron micrographs were taken at a magnification of ×8000 of NP and D18 cervices for each genotype (n= 3 animals per genotype and time point). Distribution of collagen fibrils was measured (n=1668-3054 fibrils). Twelve bins with a 15nm range show the collagen fibril distribution in the NP and D18 cervix. An increase in the number of large diameter fibrils (above 95nm; 95-125nm range) was observed only in the *Dcn*$^{-/-}$ (NP and day18), and *Dcn*$^{-/-}$ *Bgn*$^{-/-}$ (NP and day18) mice. In contrast, the emergence of smaller diameter fibrils below 26nm (17-26nm range) was detected only the Dcn$^{-/-}$ Bgn$^{-/-}$ NP cervix.

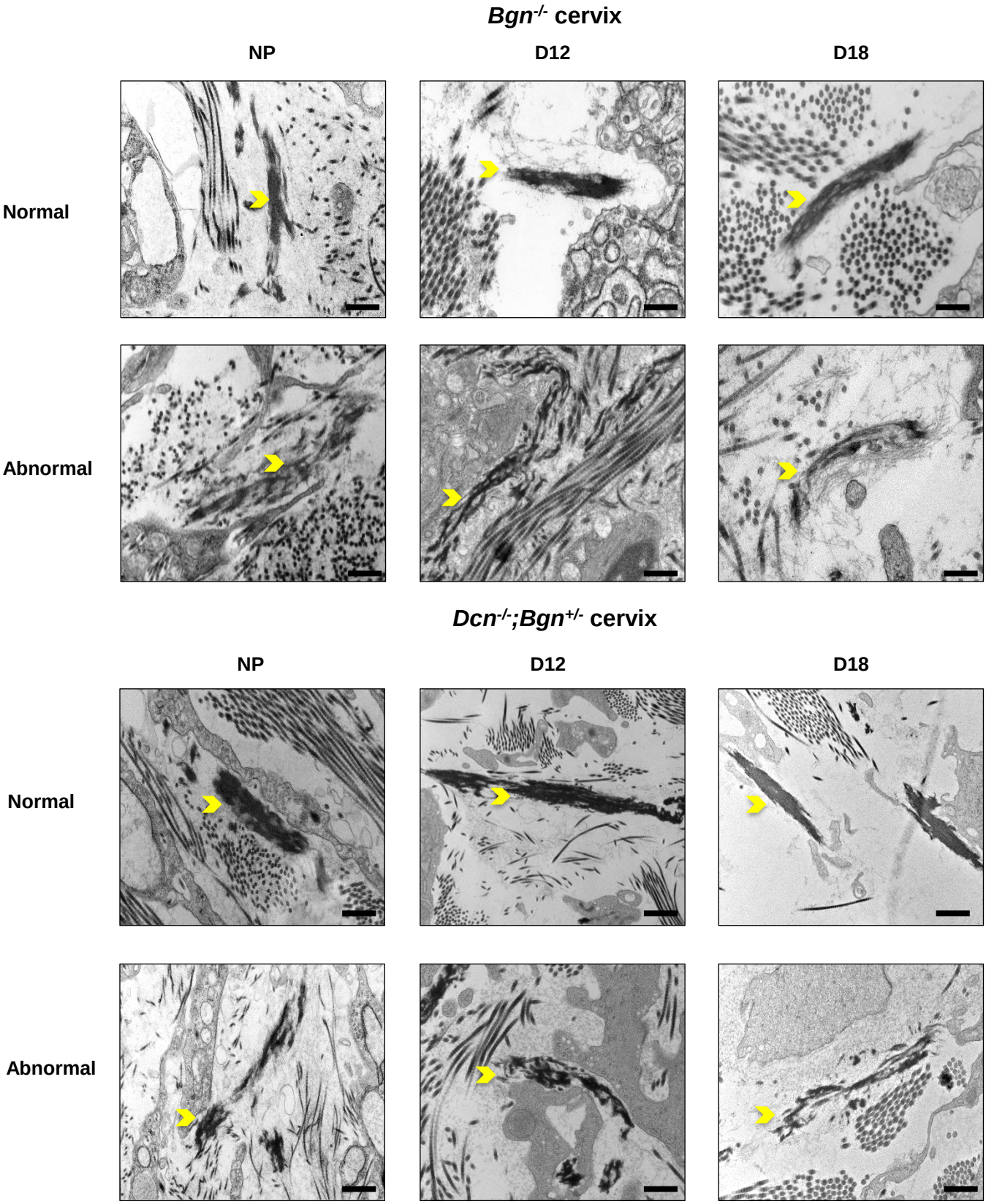

Supplementary Figure 4: A mix of normal and abnormal elastic fibers in the cervical ECM of Bgn$^{-/-}$ and Dcn$^{-/-}$;Bgn$^{+/-}$ mice. A mix of both normal and poorly assembled elastic fibers were observed in the ECM. Examples of normal and poorly assembled fibers are illustrated. The yellow arrowheads indicate elastic fibers. n= 3 animals per genotype and time point. Scale bars, 500 nm.

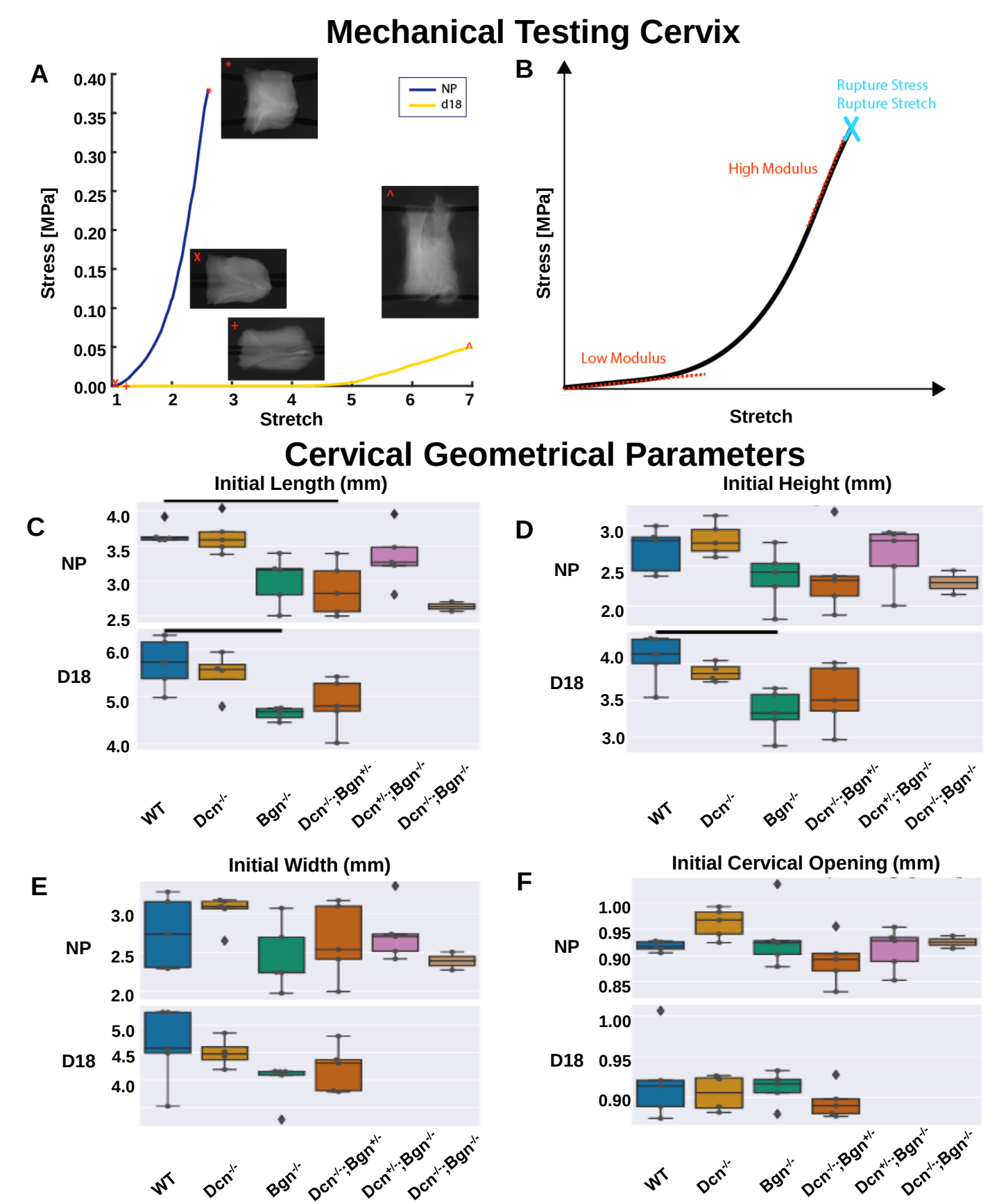

Supplementary Figure 5: Load-to-failure mechanical test of whole cervix samples designed to measure stiffness and rupture properties. A representative stress-stretch response of a NP and d18 sample to the load-to-failure test. Inset images are pictures of a NP and d18 sample at the start of the mechanical test and right before rupture (panel A). Schematic to define the calculation of four mechanical parameters using the stress-stretch curve (panel B). Initial cervical geometry measurements from the first image taken after 3hr of swelling at the start of the mechanical test (panel C-F). Overlaid dots indicate each sample. Diamonds indicate samples outside 1.5IQR. Solid lines indicate statistically significant differences between two groups ($p<0.05$).

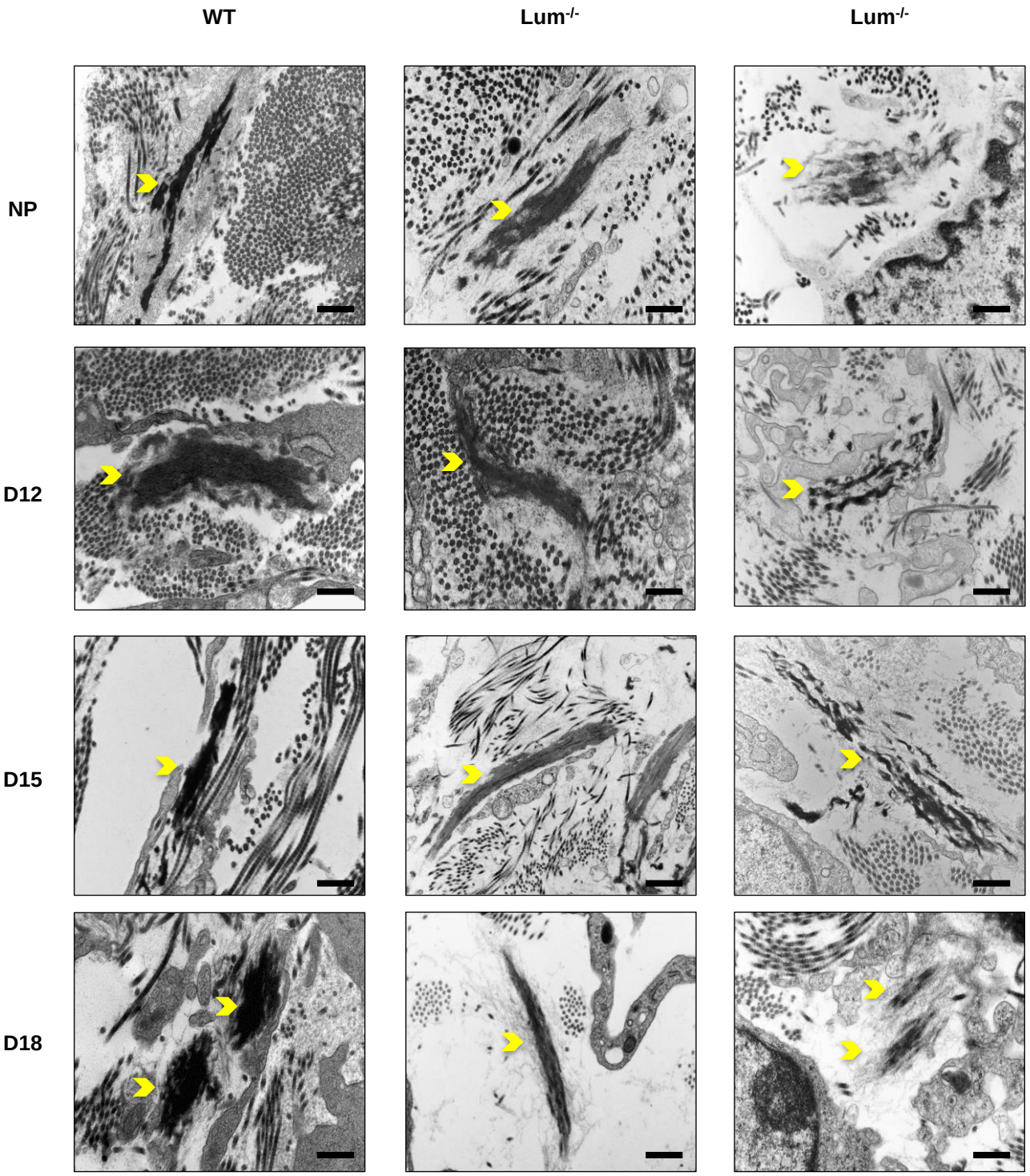

Supplementary Figure 6: A mix of normal and abnormal elastic fiber are present in cervix of Lum$^{-/-}$ during pregnancy. A mix of both normal and poorly assembled elastic fibers (yellow arrowheads) were observed in the ECM. Middle panel depicts normal fibers and panel to the right indicate poorly assembled fibers. n= 3 animals per genotype and time point. Scale bars, 500 nm.

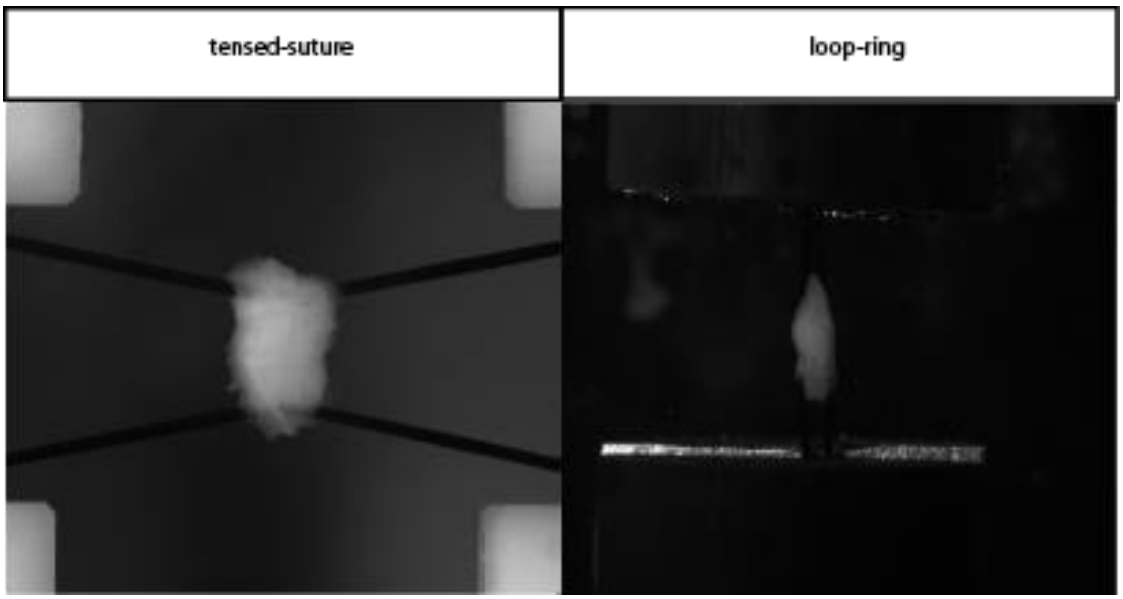

Supplementary Figure 7: Tensed-suture load vs, loop-ring load configuration. Example images of cervices right before rupture in the tensed-suture load-to-failure and loop-ring load-to-failure mechanical test configuration. The tensed-suture better controls for and minimizes the deformation of the cervix perpendicular to the desired direction of loading.

Supplementary Table 1: Measurement of collagen fibril spacing in the cervix of nonpregnant and day 18 pregnant mice

	Fibril Spacing (mean ±SEM)	p-value
Comparisons NP vs D18		
WT NP vs. WT D18	78.86nm ± 1.69 vs 104.0nm ± 2.40	<0.0001
$Dcn^{-/-}$ NP vs. $Dcn^{-/-}$ D18	91.11nm ± 2.22 vs 113.9nm ± 2.14	<0.0001
$Bgn^{-/-}$ NP vs. $Bgn^{-/-}$ D18	93.44nm ± 2.15 vs 109.6nm ± 2.10	0.0004
$Dcn^{-/-}$;$Bgn^{-/-}$ NP vs. $Dcn^{-/-}$;$Bgn^{-/-}$ D18	111.5nm ± 9.16 vs 128.0nm ± 5.63	NS
$Lum^{-/-}$ NP vs. $Lum^{-/-}$ D18	102.3nm ± 3.07 vs 99.55nm ± 1.84	NS
Comparisons between genotypes NP cohort		
WT vs. $Dcn^{-/-}$	78.86nm ± 1.69 vs 91.11nm ± 2.22	0.0011
WT vs. $Bgn^{-/-}$	78.86nm ± 1.69 vs 93.44nm ± 2.15	0.0008
WT vs. $Dcn^{-/-}$;$Bgn^{-/-}$	78.86nm ± 1.69 vs 111.5nm ± 9.16	0.0002
WT vs. $Lum^{-/-}$	78.86nm ± 1.69 vs 102.3nm ± 3.07	<0.0001
Comparisons between genotypes D18 cohort		
WT vs. $Dcn^{-/-}$	104.0nm ± 2.40 vs 113.9nm ± 2.14	NS
WT vs. $Bgn^{-/-}$	104.0nm ± 2.40 vs 109.6nm ± 2.10	NS
WT vs. $Dcn^{-/-}$;$Bgn^{-/-}$	104.0nm ± 2.40 vs 128.0nm ± 5.63	0.0057
WT vs. $Lum^{-/-}$	104.0nm ± 2.40 vs 99.55nm ± 1.84	NS